Construction and Building Materials 398 (2023) 132509

Contents lists available at ScienceDirect

Construction and Building Materials

journal homepage: www.elsevier.com/locate/conbuildmat

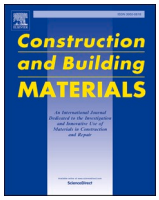

Unveiling the underlying mechanisms of tensile behaviour enhancement in fibre reinforced foam concrete

Jiehong Li, Yang Yu, Taehwan Kim, Ailar Hajimohammadi *

Centre for Infrastructural Engineering and Safety, School of Civil and Environmental Engineering, The University of New South Wales, Australia

ARTICLE INFO

Keywords:
Foam concrete
PVA fibre
Splitting tensile strength
Flexural tensile behaviour
Fibre failure mode

ABSTRACT

Fibre reinforcement is beneficial to control crack behaviour and the energy absorption ability of foam concrete. Several studies have investigated the flexural tensile behaviour of fibre-reinforced foam concrete to determine its ultimate peak strength gain. However, there remains a knowledge gap regarding the underlying mechanism of fibre influence on its tensile behaviour, as well as the impact of fibres on the pre and post-crack behaviour of foam concrete. This paper analysed and compared the flexural tensile behaviour and splitting tensile strength of PVA fibre-reinforced foam concrete. In addition, machine learning technology was used to develop regression models that described the importance of design parameters (foam concrete density, fibre length, diameter, and content), fibre distribution, and pore structure on foam concrete's tensile behaviour. The results show that the mechanism of fibre influence on pre-crack and post-crack flexural behaviour in foam concrete differs from that in normalweight concrete. In particular, contrary to the behaviour observed in normalweight concrete, PVA fibres noticeably enhanced the pre-crack flexural performance and splitting tensile strength of foam concrete. This paper found that this improvement is related to the effect of fibres on the pore structure in foam concrete, which in turn had a substantial impact on both pre-crack flexural behaviour and splitting tensile strength. Different from pre-crack behaviour (mainly influenced by pore structure), fibre content and size dominated post-crack behaviour of foam concrete. Optimising fibre size and content resulted in substantial improvements in splitting tensile strength (up to 75.3% for high-density foam concrete and 49.9% for low-density foam concrete) and flexural strength (up to 44.4% for high-density foam concrete and 117.9% for low-density foam concrete).

1. Introduction

Foam concrete is a kind of lightweight concrete without coarse aggregate, with a density ranging from 400 to 1850 kg/m^3 [1]. Due to its low density, low thermal conductivity, and high fire resistance, foam concrete has gained increased attention in recent times [2]. Density is a critical parameter that affects the strength of foam concrete [3]. Therefore, foam concrete has lower density and strength compared to normalweight concrete. Short fibres have been found to be beneficial in improving the mechanical properties of foam concrete [4–9]. It was reported that the addition of 0.4% (by volume) polypropylene (PP) fibres enhanced the compressive strength of foam concrete by 35% [10].

In concrete, fibres can act as crack bridges and prevent further crack propagation [11–14]. Consequently, fibre reinforcement is frequently employed to enhance concrete's tensile properties [15]. The addition of polypropylene (PP) fibres has been shown to increase the splitting tensile strength and flexural strength of foam concrete by 44% and 40%, respectively [16]. Amran et al. [17] also found that PP fibre improved the flexural strength of foam concrete by 49%. In addition to PP fibres, polyvinyl alcohol (PVA) fibres are advantageous for improving foam concrete's tensile behaviour due to their high modulus and strength, low cost [18], and strong bond with cementitious matrix [19]. Limited studies confirm the benefits of PVA fibres in foam concrete applications. Raj et al. [20] found that the addition of 0.3% (by volume) PVA fibre increased foam concrete's splitting tensile strength and flexural strength by 27% and 76%, respectively. Furthermore, it was reported that the flexural strength of foam concrete improved by 151.4% with the inclusion of 1.5% (by volume) PVA fibres [21].

Several parameters, such as fibre size, material, and content, have a significant impact on the properties of fibre-reinforced concrete [22,23]. For instance, it has been reported that 5 mm length sisal fibres increased the flexural strength of foam concrete by 47.6%, while the improvement with 15 mm length one was only 23.8% [24]. Additionally, Bing et al. [5] discovered that PP fibres were more effective at enhancing the

* Corresponding author.
E-mail address: ailar.hm@unsw.edu.au (A. Hajimohammadi).

https://doi.org/10.1016/j.conbuildmat.2023.132509
Received 28 March 2023; Received in revised form 14 June 2023; Accepted 12 July 2023
Available online 19 July 2023

Table 1
Size of the PVA fibres.

PVA fibre	12 mm-19 μm	6 mm-19 μm	3 mm-19 μm	12 mm-200 μm
Length (mm)	12	6	3	12
Diameter (μm)	19	19	19	200

compressive strength of foam concrete at lower densities. Although the benefits of PVA fibres in foam concrete applications are well understood, the impact of several design parameters (foam concrete density, fibre length, diameter, and content) on the tensile behaviour of the PVA fibre reinforced foam concrete has not been investigated, and there are no guidelines for the selection of accurate design parameters when PVA fibres are used for the foam concrete reinforcements. Furthermore, it is well known that the post-cracking tensile behaviour and toughness of fibre-reinforced concrete are considered to be its most important properties [25]. This is the same case with PVA fibre-reinforced foam concrete used for structural components. Understanding post-crack behaviour of PVA fibre-reinforced foam concrete is crucial in determining the extent of these enhancements, which can lead to better material selection for specific applications. However, studies on the flexural tensile behaviour of PVA fibre-reinforced foam concrete have only investigated its ultimate peak strength and few studies on its pre- and post-crack behaviour have been conducted. The first part of this study thoroughly investigated the effects of key design parameters, such as fibre length, diameter, content, and foam concrete density, on the pre- and post-crack flexural tensile behaviour and splitting tensile strength of PVA fibre-reinforced foam concrete. The second part of the paper focused on the investigation of the statistical approach to evaluate the effect of microscopic properties (including fibre distribution and pore structure as cited in another paper by the authors [26]) on foam concrete's tensile behaviour.

Furthermore, using the experimental data obtained from 26 mixtures in this study, machine learning technology was employed to better comprehend how various parameters impact the tensile behaviour of foam concrete. Machine learning has become increasingly popular in recent years for predicting concrete mechanical properties, such as compressive strength [27], tensile strength [28], and flexural strength [29]. The models can be trained on different parameters, such as the concrete mix composition, curing time, and environmental conditions. Regression algorithms, including linear regression, decision trees, artificial neural networks (ANN), and support vector machine (SVM), are commonly used in these applications [30]. The accuracy of predictions can be improved by gathering significant amounts of data and using sophisticated models. Yu, et al. [31] utilised SVM to develop a surrogate model for compressive strength prediction of high-performance concrete, where a large dataset was employed for model training and validation. Nguyen, et al. [32] developed an ANN-based model for evaluating the reduction of modulus of elasticity of concrete due to alkali-silica reaction (ASR), in which 11 influencing parameters were considered. The similar method was also applied to the compressive strength of foam concrete, where an improved firefly algorithm was used to optimise the network weights and bias to enhance the generalisation capacity [33]. Among these machine learning methods, this paper selected Gaussian process regression (GPR) to develop regression models and statistically interpret the impact of various design parameters and microscopic properties (fibre distribution and pore structure) because GPR has demonstrated superiority in nonlinear modelling of high-dimensional data [34].

2. Materials and experiment design

Portland cement, Sydney sand, water, foam, and PVA fibres were used as raw materials to produce foam concrete. The foam was generated via a synthetic-based foaming agent (ISOCEM-S/X), which was supplied by ISOLTECH. To produce the foam, a 2.5% solution of the foaming agent was aerated using compressed air and a DEMA foaming machine [35]. By regulating the solution and air flow through the nozzle, the foam density was maintained at approximately 70 kg/m^3 during the experimentation phase. Furthermore, PVA fibres of varying sizes (as detailed in Table 1) were utilized in this study, with their physical characteristics presented in Table 2. The PVA fibres were procured from Kuraray, Japan.

Standard concrete mixers are not suitable for mixing foam concretes owing to the absence of vertical motion of the matrix, which triggers the ascension of foam. As a result, a drill mixer, operating at 500 rpm, was employed to mix the foam concrete in a plastic container. The fibres were initially mixed with water, followed by the sequential addition of cement and sand during the mixing process. Finally, the pre-produced foam was added and mixed until the homogenous mixture was obtained.

A total of twenty-six sample groups, with varying fibre lengths (3, 6, and 12 mm), fibre diameters (19 and 200 μm), fibre content (ranging from 0% to 0.9% by volume), and concrete densities (800 and 1700 kg/m^3) were subjected to testing, as presented in Table 3. For example, group 1700–12-19–0.3 indicates the 1700 kg/m^3 foam concrete with 0.3% of fibres (12 mm length and 19 μm diameter). The cement, sand, and water mass ratio for all sample groups was maintained at 1:0.4:0.4. Thus, 1 m^3 of the high-density foam concrete (1700 kg/m^3) required 935 kg/m^3 of cement, 374 kg/m^3 of sand, 374 kg/m^3 of water, and 17 kg/m^3 of foam. Corresponding cement, sand, water, and foam contents for 1 m^3 of the low-density foam concrete were, respectively, 420 kg/m^3, 168 kg/m^3, 168 kg/m^3 and 44 kg/m^3.

3. Methodology and experimental techniques

Fig. 1 illustrates the methodology employed in this study. Initially, the splitting tensile strength (STS) and flexural behaviour, including first-crack flexural strength (FCS), post-crack flexural strength (PCS), and toughness (TGH), of the fibre-reinforced foam concrete were evaluated across different fibre contents (FC), aspect ratios (AR), and foam concrete densities (FD). Subsequently, a GPR model was implemented to investigate the relationship between the input parameters and the evaluated properties, while also ranking the importance of each input parameter with respect to the analysed properties. The input properties, such as the fibre dispersion coefficient (FDC), pore shape factor (PSF), pore dispersion coefficient (PDC), and D_{90}, were adopted from another paper by the authors [26] and were detailed in Section 5. Furthermore, to better comprehend how the input parameters influenced the output properties, the fibre failure mode during flexural testing was examined using scanning electron microscopy (SEM) and flexural force–displacement curves were analysed.

3.1. Splitting tensile strength

The STS test was conducted in accordance with ASTM C496/C496M-17 [36] utilizing the Shimadzu compression machine. For each group, three 100 mm × 200 mm cylinders were fabricated, and following casting, the specimens were de-moulded after a day, enveloped in cling

Table 2
Physical properties of the PVA fibres.

Fibre name	Density (g/cm^3)	Modulus of elasticity (cN/dtex)	Tensile strength (MPa)	Ultimate tensile strain (%)
PVA	1.3	380	1400–1600	6

Table 3
Mix design for foam concretes (the weight ratio of the cement, sand, and water is constant at 1:0.4:0.4 for all mixes).

Mix No.	Fibre content by volume (%)	Fibre length (mm)	Fibre diameter (μm)	Foam Concrete density (kg/m^3)
Control (1700)	0	N/A	N/A	1700
1700-12-19-0.3	0.3	12	19	1700
1700-12-19-0.6	0.6	12	19	1700
1700-12-19-0.9	0.9	12	19	1700
1700-6-19-0.3	0.3	6	19	1700
1700-6-19-0.6	0.6	6	19	1700
1700-6-19-0.9	0.9	6	19	1700
1700-3-19-0.3	0.3	3	19	1700
1700-3-19-0.6	0.6	3	19	1700
1700-3-19-0.9	0.9	3	19	1700
1700-12-200-0.3	0.3	12	200	1700
1700-12-200-0.6	0.6	12	200	1700
1700-12-200-0.9	0.9	12	200	1700
Control (800)	0	N/A	N/A	800
800-12-19-0.05	0.05	12	19	800
800-12-19-0.15	0.15	12	19	800
800-12-19-0.3	0.3	12	19	800
800-6-19-0.05	0.05	6	19	800
800-6-19-0.15	0.15	6	19	800
800-6-19-0.3	0.3	6	19	800
800-3-19-0.05	0.05	3	19	800
800-3-19-0.15	0.15	3	19	800
800-3-19-0.3	0.3	3	19	800
800-12-200-0.3	0.3	12	200	800
800-12-200-0.6	0.6	12	200	800
800-12-200-0.9	0.9	12	200	800

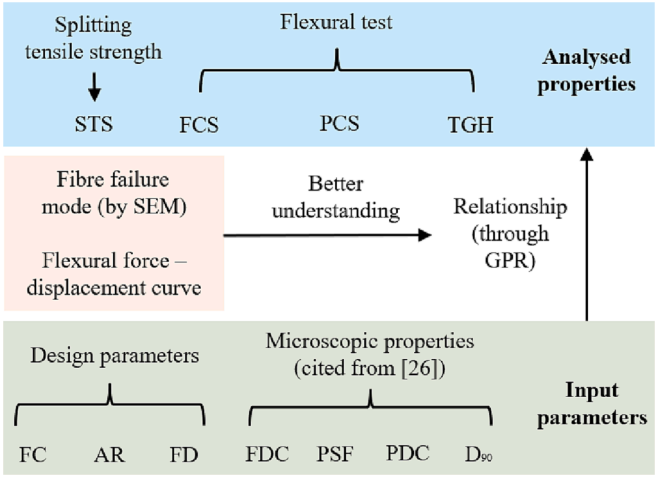

Fig. 1. Framework of the methodology for the analysis.

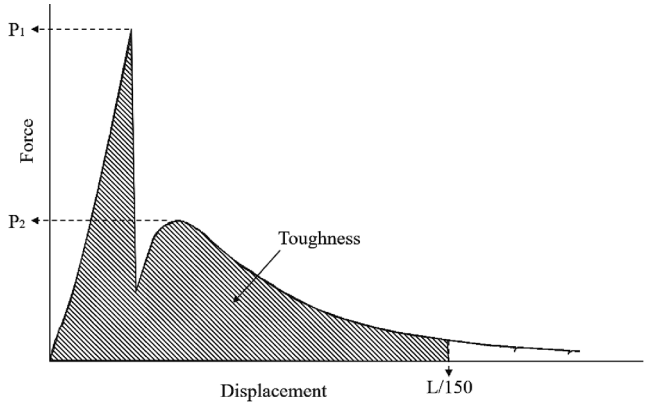

Fig. 2. Example of the force–displacement curve for fibre-reinforced foam concrete (not to scale).

wrap, and cured for 27 additional days in a curing room at 23 ℃ prior to testing. The results presented represent the average outcomes of these three samples.

3.2. Flexural tensile behaviour

The flexural tests were conducted in accordance with ASTM C348-19 [37]. Each group consisted of three replicate prisms (40 × 40 × 160 mm). The curing method and duration were identical to that of the STS test. The central point bending test was executed utilising an Instron machine. Furthermore, a displacement gauge was employed to measure the central displacement of the sample, which facilitated the generation and analysis of a force–displacement curve.

The FCS, PCS, and TGH were evaluated from the force–displacement curve. Fig. 2 illustrates an instance of the force–displacement curve for fibre-reinforced foam concrete. The initial crack and post-crack peak forces (P_1 and P_2, respectively) were used to compute FCS and PCS. According to ASTM C348-19 [37], the overall area beneath the force–displacement curve up to a displacement equivalent to 1/150th of the span length (0.8 mm in this study) was regarded as the TGH.

3.3. Scanning electron microscopy (SEM) analysis

A TM4000Plus SEM was used to perform SEM analysis and examine the fibre failure mode in foam concrete under tensile stress. After the flexural test, the prism was bisected at the midpoint, resulting in two fracture surfaces. A 10 mm-sided cube was obtained by sampling the lower centre of any fracture surface for SEM analysis, ensuring that the fracture surface remained intact throughout the sampling process. The cube fragment was glued on the sample holder and then sputter-coated with carbon. The analysis was carried out under the vaccume condition using 15 kV of accelerating voltage. The SEM images acquired from the fracture surfaces illustrated how the fibres failed during the flexural test. Furthermore, the fibre failure mode was investigated to infer the degree of bonding of the fibres to the foam concrete.

Table 4
Splitting tensile strength (STS) and flexural behaviour (FCS, PCS and TGH) of the foam concrete. Results show the average test result of three specimens and SD is the standard deviation.

Mix No.	STS (MPa)	SD	FCS (MPa)	SD	PCS (MPa)	SD	TGH (J)	SD
Control (1700)	1.74	0.026	4.05	0.110	N/A	N/A	0.092	0.001
1700-12-19-0.3	2.72	0.029	4.67	0.121	2.07	0.065	0.332	0.016
1700-12-19-0.6	2.53	0.019	4.04	0.032	3.91	0.145	0.604	0.003
1700-12-19-0.9	2.3	0.072	3.33	0.151	4.72	0.127	0.761	0.005
1700-6-19-0.3	2.64	0.018	4.76	0.105	2.4	0.175	0.35	0.012
1700-6-19-0.6	2.7	0.025	5.04	0.325	4.19	0.041	0.611	0.012
1700-6-19-0.9	2.64	0.043	4.62	0.083	5.85	0.023	0.9	0.026
1700-3-19-0.3	2.63	0.063	4.75	0.061	2	0.042	0.288	0.006
1700-3-19-0.6	2.8	0.031	4.82	0.030	4.06	0.064	0.56	0.010
1700-3-19-0.9	3.05	0.042	5.22	0.280	5.47	0.155	0.771	0.027
1700-12-200-0.3	2.28	0.109	4.25	0.111	N/A	N/A	0.105	0.020
1700-12-200-0.6	2.32	0.088	4.42	0.024	1.74	0.044	0.41	0.010
1700-12-200-0.9	2.5	0.009	4.54	0.045	2.57	0.015	0.667	0.007
Control (800)	0.363	0.010	0.624	0.016	N/A	N/A	0.015	0.001
800-12-19-0.05	0.42	0.005	0.687	0.005	0.294	0.092	0.056	0.004
800-12-19-0.15	0.434	0.006	0.86	0.075	0.774	0.114	0.149	0.027
800-12-19-0.3	0.277	0.003	0.627	0.005	0.875	0.005	0.181	0.012
800-6-19-0.05	0.477	0.015	0.795	0.025	0.347	0.032	0.073	0.001
800-6-19-0.15	0.544	0.009	1.068	0.037	1.019	0.070	0.183	0.009
800-6-19-0.3	0.414	0.009	0.987	0.045	1.361	0.068	0.287	0.007
800-3-19-0.05	0.423	0.012	0.665	0.005	0.312	0.003	0.071	0.003
800-3-19-0.15	0.448	0.004	0.857	0.010	0.762	0.029	0.145	0.010
800-3-19-0.3	0.382	0.008	0.793	0.011	0.953	0.071	0.212	0.011
800-12-200-0.3	0.436	0.004	0.76	0.041	0.563	0.083	0.149	0.021
800-12-200-0.6	0.444	0.004	1.027	0.051	1.061	0.040	0.257	0.013
800-12-200-0.9	0.51	0.007	1.04	0.013	1.315	0.065	0.312	0.002

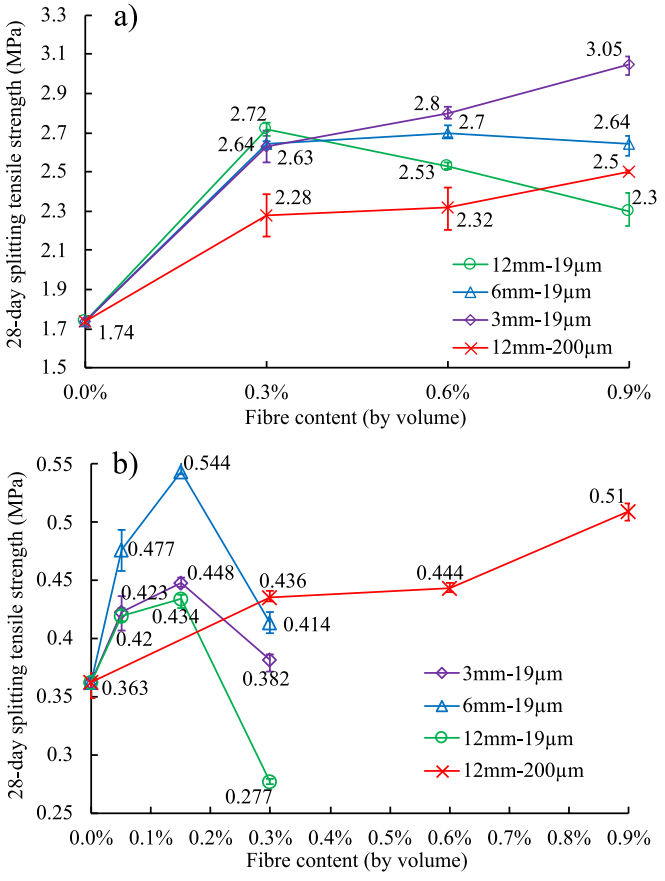

Fig. 3. Splitting tensile strength of the foam concrete with densities of a) 1700 kg/m^3 and b) 800 kg/m^3.

4. Results

This section presents the results of the STS and flexural tensile behaviour (FCS, PCS and TGH) of foam concrete, along with SEM analysis of the fibre failure mode during the flexural test. All experimental results from this research, including STS, FCS, PCS, and TGH, are presented in Table 4. These results were elaborated on in subsequent parts of this section and were further discussed in Section 5.

4.1. Splitting tensile strength

Fig. 3a presented the STS of 1700 kg/m^3 foam concrete as a function of fibre content and the fibre properties (length and diameter). The performance of 3 mm-19 μm fibres was the most effective for the improvement in STS, which incorporating 0.9% of these fibres resulted in a 75.3% increase in STS. On the other hand, the addition of 12 mm-19 μm and 6 mm-19 μm fibres initially increased STS, but STS decreased when beyond an optimal content. Fibres with a diameter of 200 μm were found to be less effective than their 19 μm counterparts. Nonetheless, similar to the 3 mm-19 μm fibres, the STS continued to increase with the addition of more 200 μm diameter fibres.

Fig. 3b presents the STS of 800 kg/m^3 foam concrete. Notably, an increase in STS was observed with an increasing content (up to 0.15%) of 19 μm diameter fibres. Among all the fibres tested, 0.15% of 6 mm-19 μm fibres exhibited the best performance, resulting in a 49.9% enhancement in STS. However, STS decreased with a higher fibre content of 19 μm diameter fibres. For instance, incorporating 0.3% of 12 mm-19 μm fibres decreased the STS of foam concrete by 23.7%. On the other hand, STS continued to increase with the addition of 200 μm diameter fibres. Using 0.9% of 12 mm-200 μm fibres resulted in a 40.5% increase in STS.

It has been reported that the integration of micro-PVA fibres resulted in an enhancement of up to 32% in the STS of normalweight concrete [38]. Compared to normalweight concrete, PVA fibres are more effective in enhancing the STS of foam concrete, with improvements of up to 75.3% and 49.9% observed in high-density and low-density foam concrete, respectively. Unlike the normalweight concrete, foam concrete has pore structures genereated by the addition of foam and the previous

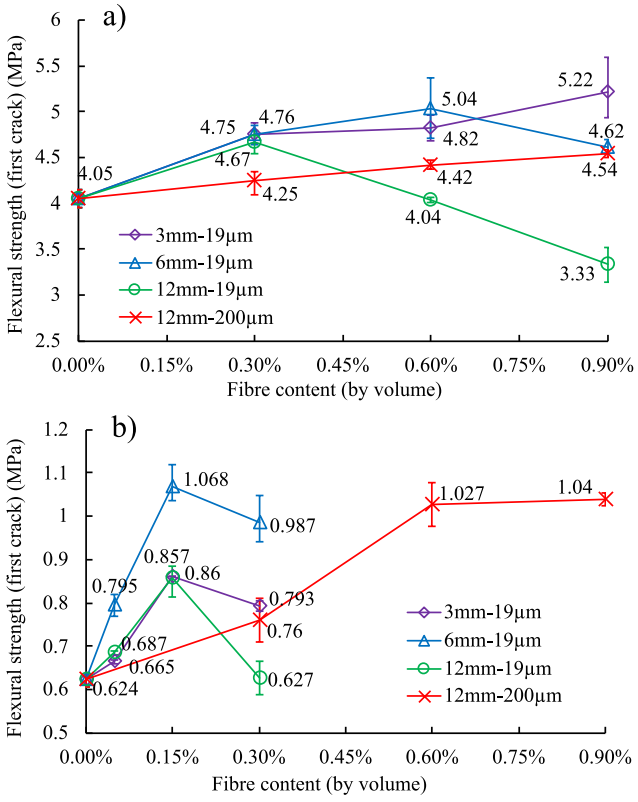

Fig. 4. Flexural strength (based on the first-crack force) of the foam concrete with densities of a) 1700 kg/m^3 and b) 800 kg/m^3.

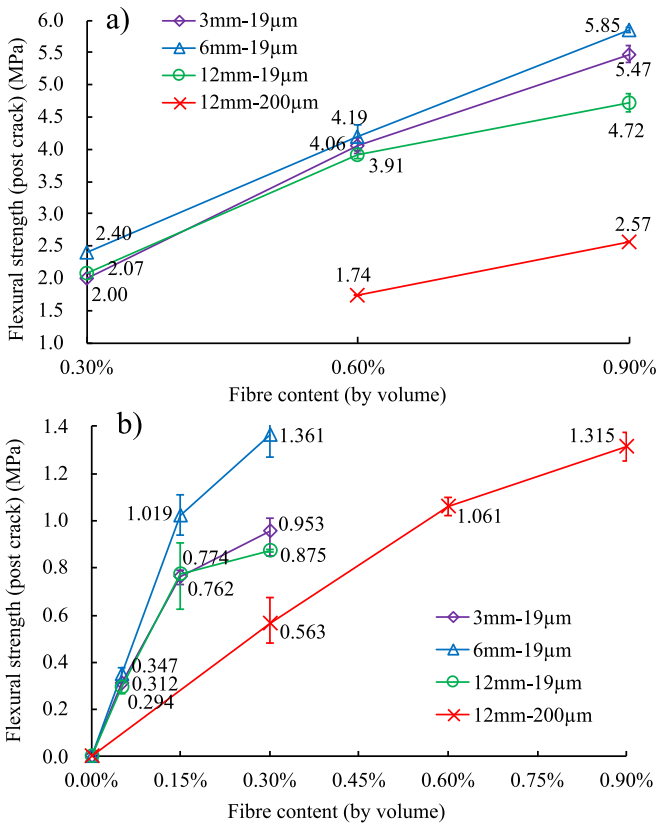

Fig. 5. Flexural strength (based on the peak residual load) of the foam concrete with densities of a) 1700 kg/m^3 and b) 800 kg/m^3.

study [26] revealed that the fibre affected these pore structures. More details of the underlying mechanisms of fibre contributing to the tensile behaviour of foam concrete will be discussed in Section 5.2.

4.2. *Flexural tensile behaviour*

This section explores the 28-day flexural tensile behaviour of foam concrete with densities of 1700 kg/m^3 and 800 kg/m^3, covering its FCS, PCS, TGH, and force–deflection response. Additionally, SEM images depicting the fibre failure mode during the flexural test are provided.

Fig. 4a displays the FCS of 1700 kg/m^3 foam concrete. The results show that incorporating 0.9% of 3 mm-19 μm fibres led to the most significant improvement (a 28.9% increase) in FCS. Both the 12 mm-19 μm and 6 mm-19 μm fibres were also effective in enhancing the FCS. However, exceeding the optimal fibre content had a negative influence on most of the sample groups. In Fig. 4b, the FCS of 800 kg/m^3 foam concrete is shown. The findings indicate that 6 mm-19 μm fibres performed best in 800 kg/m^3 foam concrete, with 0.15% of such fibres enhancing the FCS by 71.2%. Additionally, 0.15% was identified as the optimal content for 19 μm diameter fibres, and with higher fibre content leading to a negative influence. Unlike the behaviour of 19 μm diameter fibres, the FCS continued to increase with the increase of the content of 200 μm diameter fibres. The addition of 0.9% of 12 mm-200 μm fibres resulted in a 66.7% increase in the FCS. It was reported that a low content of micro-PVA fibres (less than 2% by volume) shows limited improvements to the FCS of normalweight concrete [39]. This observation markedly contrasts with the behaviour of foam concrete. As demonstrated in Fig. 4, PVA fibres considerably strengthen the FCS of the foam concrete. The underlying factors contributing to this difference were discussed in Section 5.2.

Fig. 5 presents the PCS of the foam concrete. Notably, no PCS was observed for the 1700 kg/m^3 foam concrete with 0.3% of 12 mm-200 μm fibres (as shown in Fig. 5a). This is because the force dropped rapidly to zero after the specimen cracked, causing the machine to stop working. Based on Fig. 5, the PCS increased with the increase in fibre content. The foam concrete with 200 μm diameter fibres exhibited lower PCS than that with 19 μm diameter fibres under the same fibre content. Among the 19 μm diameter fibres, the 6 mm length fibres exhibited the best performance. When the flexural strength was calculated using the ultimate peak force, the 6 mm-19 μm fibres enhanced the flexural strength of the 1700 kg/m^3 and 800 kg/m^3 foam concrete by up to 44.4% and 117.9%, respectively. In contrast, the 12 mm-19 μm fibres provided the lowest improvement for the PCS of both 1700 kg/m^3 and 800 kg/m^3 foam concrete compared with other 19 μm diameter fibres.

Fig. 6 displays the TGH of the foam concrete. The incorporation of fibres significantly improved the TGH of the foam concrete, and the TGH increased with the increase in fibre content. Foam concrete with 200 μm diameter fibres exhibited lower TGH than 19 μm diameter fibres under the same fibre content. Based on Fig. 6, a fibre length of 6 mm was deemed optimal for 19 μm diameter fibres, improving the TGH of the 1700 kg/m^3 and 800 kg/m^3 foam concrete by up to 878.3% and 1813.3%, respectively.

Fig. 7 displays the force–deflection responses of 1700 kg/m^3 foam concrete with 12 mm-19 μm and 12 mm-200 μm fibres. The force–deflection curves of the foam concrete with other 19 μm diameter fibres are relatively similar, varying only in peak values and are, therefore, not presented in this paper. Three specimens were tested for each group, and the one closest to the mean value is depicted in Fig. 7. As illustrated in Fig. 7a, for the 1700 kg/m^3 foam concrete with 19 μm diameter fibres, the force rapidly declined after cracking, then began to rise and reached the post-crack peak value, and finally dropped until the end of the experiment. With a high content of fibres, the specimens showed strain-hardening behaviour, and the post-crack peak force exceeded the first-crack force. In contrast, for the 1700 kg/m^3 foam concrete with 200 μm diameter fibres, the force gradually increased after cracking and

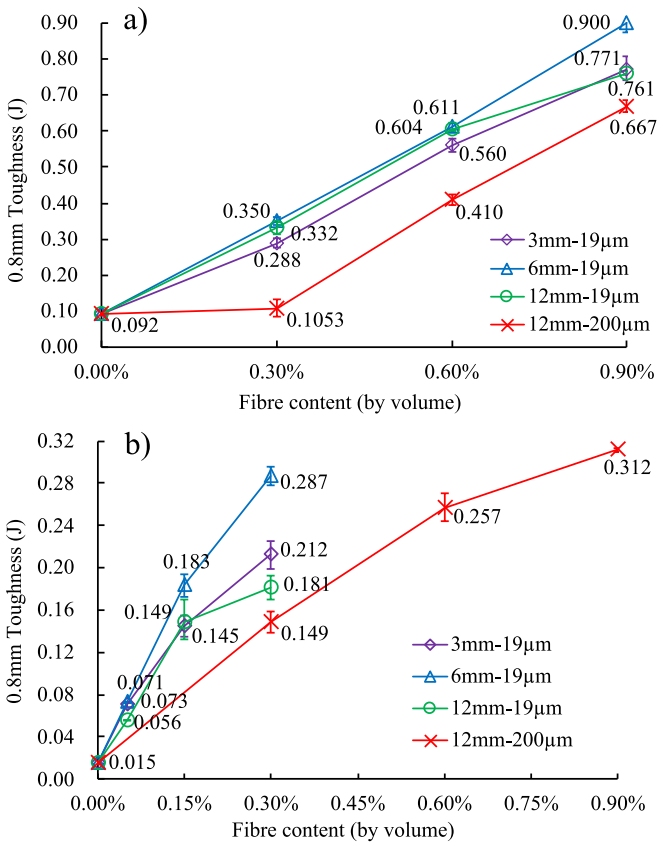

Fig. 6. Flexural toughness of the foam concrete with densities of a) 1700 kg/m^3 and b) 800 kg/m^3.

remained much lower than the first-crack force until the end of the experiment (as shown in Fig. 7b). As mentioned in the previous paragraph and shown in Fig. 5a, there was no post-crack response for the 1700 kg/m^3 foam concrete with 0.3% of 200 μm diameter fibres as the machine stopped working when the first crack occurred.

Fig. 8 presents the force–deflection responses of 800 kg/m^3 foam concrete (with the specimen closest to the mean value displayed). As shown in Fig. 8a, for the 800 kg/m^3 foam concrete with 19 μm diameter fibres, the force–displacement curve trend was similar to the 1700 kg/m^3 foam concrete, with the force increasing after cracking until the post-crack peak value. In contrast, for the 800 kg/m^3 foam concrete with 200 μm diameter fibres, the specimens exhibited strain-hardening behaviour at high fibre content (as shown in Fig. 8b), which differed from the behaviour of the 1700 kg/m^3 foam concrete.

All specimens in this research exhibited only a single crack during the flexural test. For instance, Fig. 9 shows the crack observed in samples from the 1700–6-19–0.9 and 800–6-19–0.3 groups at a displacement of 0.8 mm. The potential factors contributing to this phenomenon were discussed in Section 5.

4.3. SEM analysis

This section includes SEM analysis conducted to investigate the fibre failure mode (pull-out or rupture). Fibre rupture indicates that the bond strength between the fibres and matrix was greater than the fibres' tensile strength. Furthermore, the pull-out length of the ruptured fibres was examined and compared, with longer pull-out lengths indicating lower bond strength between the fibres and matrix. Additionally, the morphology of the pull-out fibres' surface was analysed.

4.3.1. SEM images of 1700 kg/m^3 foam concrete

Fig. 10 presents the SEM images of 1700 kg/m^3 fibre-reinforced foam concrete. The 200 μm diameter fibres showed pull-out failure in the 1700 kg/m^3 foam concrete bending test. As illustrated in Fig. 10a, the 200 μm diameter fibre was partially damaged during the pull-out process, indicating a sliding interface between the fibre and cementitious matrix. This finding confirms that the bond strength between the 200 μm diameter fibre and matrix was lower than the strength of the matrix itself. Therefore, enhancing the bond strength of 200 μm diameter fibres can improve the mechanical properties of 1700 kg/m^3 foamed concrete.

Conversely, the 19 μm diameter fibres exhibited a little pull-out and eventual rupture in 1700 kg/m^3 foam concrete, as shown in Fig. 10b. The clean surface of the 19 μm diameter fibre shown in Fig. 10b suggests that the fibre was undamaged during the pull-out process, but the sliding frictional force was still greater than the strength of the single fibre and resulted in its rupture. Fig. 10c displays the fracture surface of the foam concrete with uniformly distributed 19 μm diameter fibres, showing relatively short fibre pull-out lengths when the fibres were uniformly distributed. However, as shown in Fig. 10d, the foam concrete with non-uniformly distributed fibres led to fibre agglomeration, decreasing matrix compactness and thus reducing the fibre bond strength while increasing the fibre pull-out length in 1700 kg/m^3 foamed concrete.

4.3.2. SEM images of 800 kg/m^3 foam concrete

Fig. 11 displays the SEM images of 800 kg/m^3 fibre-reinforced foam concrete. Similar to the 1700 kg/m^3 foam concrete, the 200 μm diameter fibres exhibited pull-out failure in the bending test of 800 kg/m^3 foam concrete. As shown in Fig. 11a, the cementitious matrix adhered to the

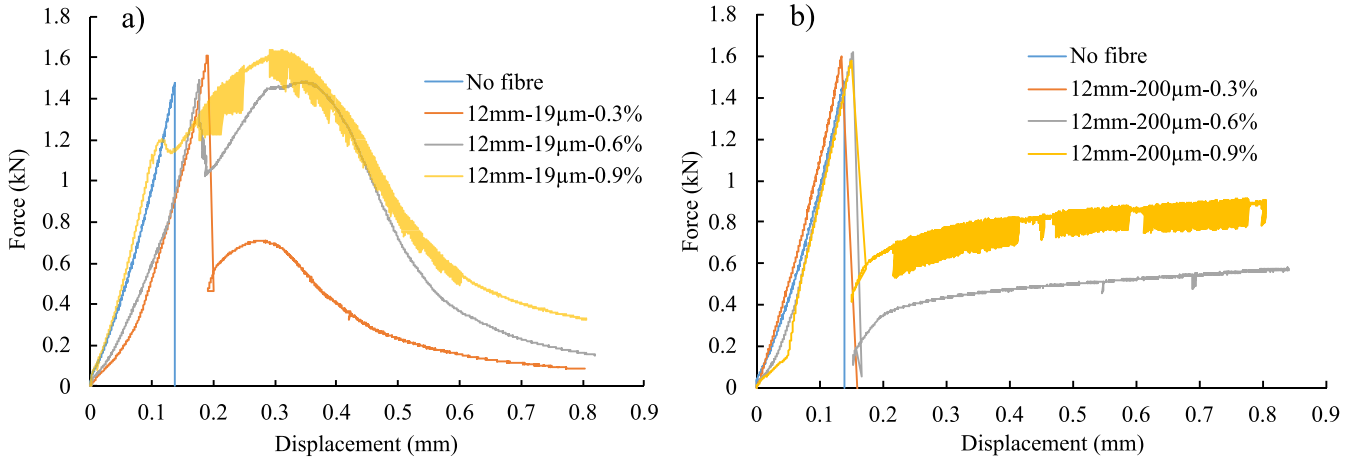

Fig. 7. Force-deflection responses of the 1700 kg/m^3 foam concrete with: a) 12 mm-19 μm fibres and b) 12 mm-200 μm fibres.

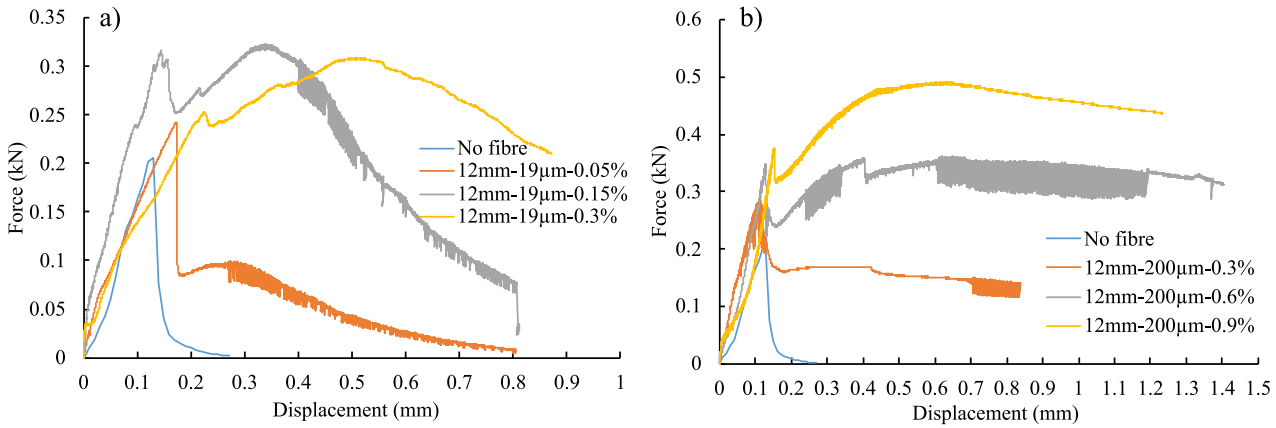

Fig. 8. Force-deflection responses of the 800 kg/m^3 foam concrete with: a) 12 mm-19 μm fibres and b) 12 mm-200 μm fibres.

Fig. 9. Examples of the samples' crack in flexural test at 0.8 mm displacement: a) 1700-6-19-0.9 and b) 800-6-19-0.3.

surface of the pulled-out 200 μm diameter fibres, indicating that most of the slippage occurred within the cementitious matrix. This confirms that the bond strength between the 200 μm diameter fibre and matrix was greater than the strength of the matrix itself. Therefore, in contrast to the case in 1700 kg/m^3, enhancing the bond strength of 200 μm diameter fibres in 800 kg/m^3 foam concrete would not be beneficial.

The 19 μm diameter fibres in the 800 kg/m^3 foam concrete exhibited a small amount of pull-out before eventually rupturing (as shown in Fig. 11b). Fig. 11c displays the fracture surface area with uniformly distributed 19 μm diameter fibres. It should be noted that the fibre pull-out length in 800 kg/m^3 foam concrete was longer than that in 1700 kg/m^3 foam concrete (as shown in Fig. 10c), indicating a lower bond strength of fibres with the higher porosity of low-density foam concrete. Based on Fig. 11d, in the non-uniform fibre distribution area, the fibre pull-out length was longer, and some matrix fragments adhered to the fibres' surface. This suggests that the non-uniform distribution of fibres reduced the fibre bond strength as well as the strength of the surrounding matrix.

5. Discussion

In this section, GPR was implemented to model the tensile behaviour of foam concrete based on various macroscopic (design parameters) and microscopic properties. Using the results of the GPR model, the importance of each parameter on the tensile behaviour of foam concrete was investigated via Shapley Additive explanations (SHAP).

The microscopic properties of the foam concrete were extracted from a previous publication by the same authors [26] and are presented in Table 5. These properties comprise the FDC, PSF, PDC, and D_{90}. The FDC parameter quantifies the degree of fibre distribution, with higher values denoting more uniformly dispersed fibres. The PSF parameter characterises the pore shape regularity, with higher values denoting more regular-shaped pores. The PDC parameter measures the pore distribution uniformity, with higher values indicating a more uniform distribution of pores. The D_{90} parameter represents the 90th percentile of the pore size distribution, indicating that 90% of the pores are smaller than D_{90}.

5.1. Gaussian process regression (GPR) model

In GPR, the uncertainty in the output of a function is modelled as a Gaussian distribution, whose mean and covariance are determined by a set of basis functions and their hyperparameters. These hyperparameters are learned from data using maximum likelihood or Bayesian optimization. The resulting Gaussian process can be used to make predictions for unseen input data, with the uncertainty of these predictions determined by the covariance. This approach allows GPR to model complex and non-linear relationships in the data while also providing a measure of uncertainty in the predictions. In this study, GPR is employed to establish surrogate models to evaluate the tensile behaviour of foam concrete, including STS, FCS, PCS and TGH. The inputs of four GPR models, namely GPR-STS, GPR-FCS, GPR-PCS and GPR-TGH, respectively, comprise both macroscopic and microscopic parameters of foam concrete, such as FD, FC, AR, FDC, PSF, PDC and D_{90}. All the experimental data are employed to train and validate the performance of the GPR models. The surrogate models are implemented using Matlab v.2021a Regression Learner Toolbox. To avoid the overfitting problem of trained models, 5-folder cross-validation is applied in the training procedure. In addition, to improve the generalisation capacity of GPR models, Bayesian optimisation algorithm is utilised to optimise the model hyperparameters, including basis function, kernel function, kernel scale and noise standard deviation coefficient (β), the results of which are displayed in Table 6.

Then, correlation analysis is conducted on all the GPR models to evaluate the capabilities in predicting mechanical properties of foam concrete. The relevant results are shown in Fig. 12. It is clearly observed that all four GPR models exhibit excellent performance in predicting mechanical properties of foam concrete, with R-squared values of more than 0.98. Among four models, GPR-FCS has the best capability for predicting first crack strength, with R-squared value of 0.9989, followed by GPR-STS, GPR-PCS and GPR-TGH.

5.2. The importance of input parameters

To better understand the importance of different input variables to

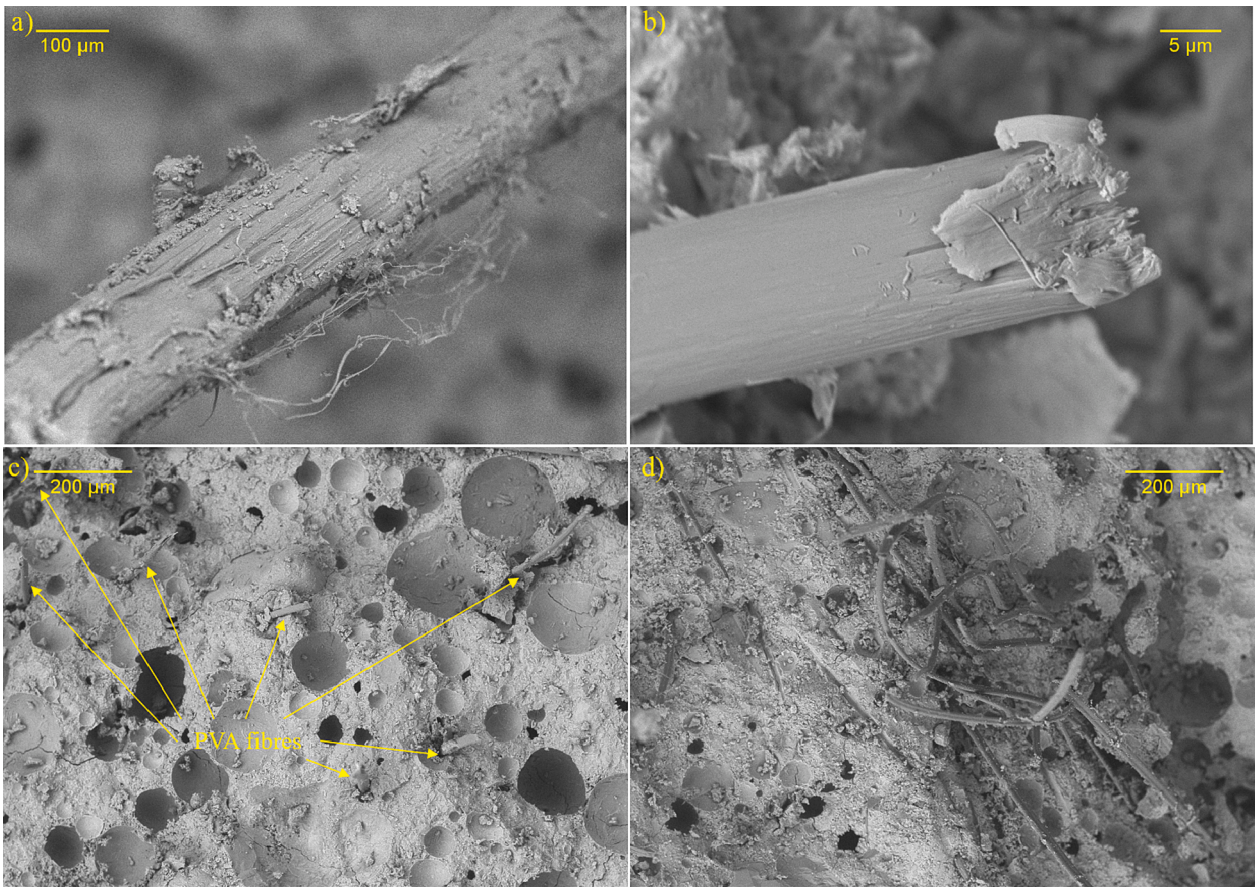

Fig. 10. SEM images of 1700 kg/m^3 fibre reinforced foam concrete (fracture surfaces of the specimens after bending test): a) surface of 200 μm diameter fibre (from 1700 to 12-200-0.6); b) surface and rupture of 19 μm diameter fibre (1700-6-19-0.3); c) the area with uniform distributed 19 μm diameter fibres (1700-6-19-0.3); and d) the area with non-uniform distributed 19 μm diameter fibres (1700-12-19-0.9).

affect the output mechanical properties, it is necessary to interpret the GPR models using SHAP. SHAP is a method for interpreting the output of machine learning models by assigning each feature an importance value for a specific prediction [40]. The method is based on the Shapley value from cooperative game theory and provides a fair and unique way to distribute the contribution of each feature to a prediction. The Shapley values account for the interactions between features and assign values based on the marginal contribution of a feature to the prediction, making it suitable for models with nonlinear relationships between features and the target. In this study, the interpretation of GPR models using SHAP is implemented by Matlab v.2021a, and the analysis results are depicted in Fig. 13.

Fig. 13a and Fig. 13b depict the input parameters' importance for STS and FCS, respectively. As pre-crack behaviour, both STS and FCS were predominantly affected by FD, D_{90}, and PSF (especially FD). In comparison to high-density foam concrete, low-density foam concrete exhibited more pores and was, therefore, more prone to cracking under stress, leading to significantly lower STS and FCS. Furthermore, larger pores were more implicated in the foam concrete's weakness [41], and thus higher D_{90} values led to decreased STS and FCS. Additionally, irregularly shaped pores (lower PSF) caused stress concentration, promoting crack initiation and development, thus reducing the foam concrete's STS and FCS.

SHAP analysis clearly indicated that the parameters related to the pore structure (D_{90} and PSF) affect the STS and FCS of the foam concrete. As explained in Sections 4.1 and 4.2, the incorporation of PVA fibres led to a substantial enhancement in the STS and FCS of the foam concrete, with increases of up to 75.3% and 71.2% respectively. These increased percentages were higher than those observed in normalweight concrete. The previous study [26] revealed that the introduction of the fibre (of suitable proportions and dimensions) into foam concrete improved the pore structure. Therefore, the significant enhancement of STS and FCS in foam concrete was the result of the pore structure improvements with the introduction of fibres (of suitable contents and sizes). Conversely, normalweight concrete, being considerably denser and less porous compared to foam concrete, derives its STS and FCS improvements solely from the fibres themselves, resulting in a more modest enhancement of STS and FCS.

Fig. 13c and Fig. 13d illustrate the input parameters' significance for PCS and TGH, respectively. As post-crack behaviour, both PCS and TGH were primarily influenced by FC, AR, and D_{90} (especially FC). As previously noted, fibres in concrete can bridge cracks and limit their further propagation [11–14]. Hence, fibres' effectiveness in improving the foam concrete's post-crack behaviour should be more pronounced than their effect on pre-crack behaviour. Therefore, FC was the principal factor influencing post-crack behaviour (PCS and TGH) but not the principal factor affecting pre-crack behaviour (STS and FCS). AR was another key factor that influenced PCS and TGH. As depicted in Fig. 5 and Fig. 6, the impact of AR on PCS and TGH was predominantly determined by fibre diameter. The lower bond strength of 200 μm diameter fibres, due to their smaller surface area, limited their effectiveness in reinforcing foam concrete for PCS and TGH compared to 19 μm diameter fibres. As shown in Fig. 10 and Fig. 11, 19 μm diameter fibres exhibited little pull-out and eventual rupture, indicating their bond force was greater than the strength of a single fibre. The high bond strength and elasticity modulus of 19 μm diameter PVA fibres led to strain-hardening behaviour (as shown in Fig. 7 and Fig. 8), resulting in high PCS and TGH of the foam concrete. Nonetheless, the fracture of 19 μm diameter fibres rendered

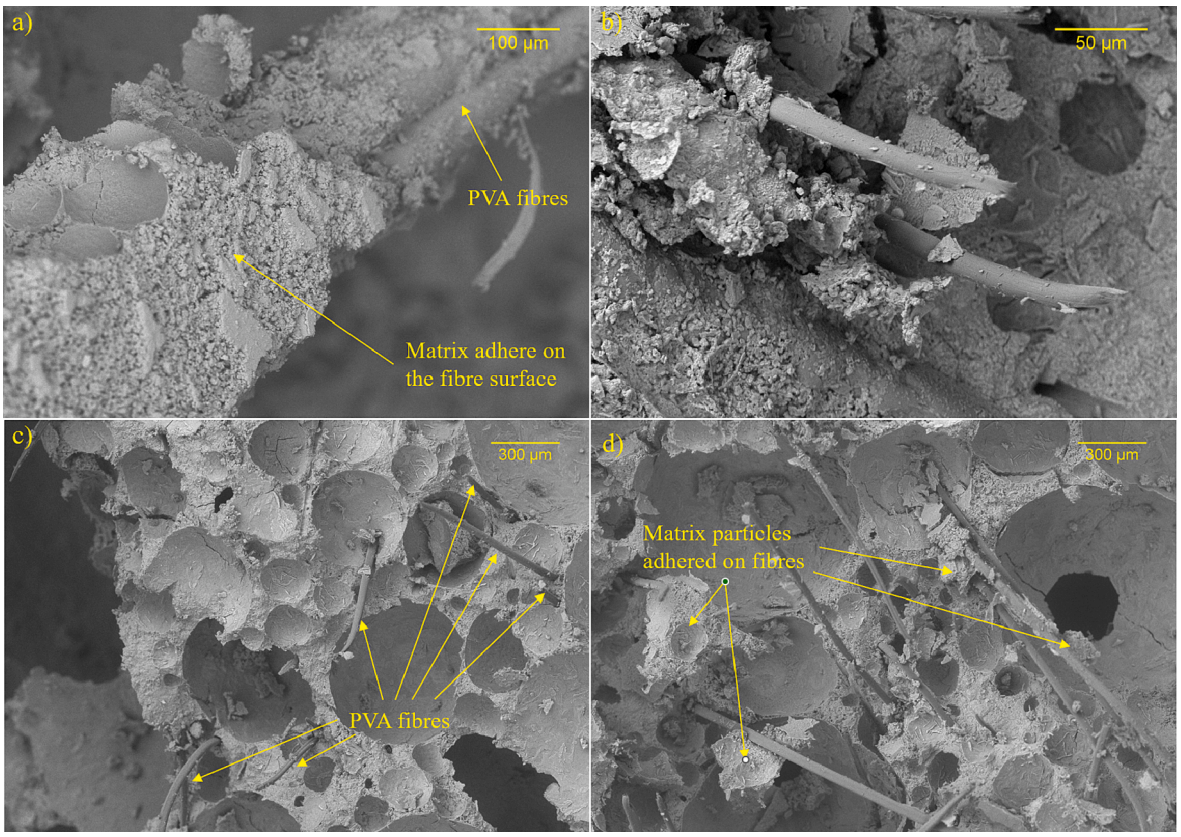

Fig. 11. SEM images of 800 kg/m^3 fibre reinforced foam concrete (fracture surfaces of the specimens after bending test): a) failure mode and surface of 200 μm diameter fibre (800-12-200-0.6); b) failure mode and surface of 19 μm diameter fibre (800-6-19-0.15); c) the area with uniform distributed 19 μm diameter fibres (800-6-19-0.15); and d) the area with non-uniform distributed 19 μm diameter fibres (800-12-19-0.3) (the fibres were close to each other or even adhered together).

Table 5
Microscopic properties of the foam concrete [26].

Mix No.	FDC	PSF	PDC	D_{90} (μm)
Control (1700)	n/a	0.814	0.397	224
1700-12-31-0.3	0.362	0.812	0.382	193
1700-12-31-0.6	0.327	0.757	0.378	233
1700-12-31-0.9	0.299	0.717	0.369	229
1700-6-31-0.3	0.386	0.844	0.393	190
1700-6-31-0.6	0.343	0.848	0.410	218
1700-6-31-0.9	0.324	0.837	0.398	210
1700-3-31-0.3	0.345	0.821	0.398	202
1700-3-31-0.6	0.337	0.839	0.381	204
1700-3-31-0.9	0.321	0.924	0.404	174
1700-12-200-0.3	0.397	0.830	0.393	208
1700-12-200-0.6	0.387	0.848	0.406	207
1700-12-200-0.9	0.358	0.9	0.398	165
Control (800)	n/a	0.81	0.436	513
800-12-31-0.05	0.312	0.768	0.441	505
800-12-31-0.15	0.272	0.711	0.426	561
800-12-31-0.3	0.258	0.667	0.408	594
800-6-31-0.05	0.349	0.81	0.437	491
800-6-31-0.15	0.331	0.815	0.456	453
800-6-31-0.3	0.298	0.781	0.427	500
800-3-31-0.05	0.351	0.828	0.449	458
800-3-31-0.15	0.310	0.777	0.434	508
800-3-31-0.3	0.279	0.754	0.428	572
800-12-200-0.3	0.372	0.823	0.427	520
800-12-200-0.6	0.359	0.815	0.449	517
800-12-200-0.9	0.349	0.807	0.457	525

them ineffective, causing the force (in the bending test) to decline rapidly after the post-crack peak value (as depicted in Fig. 7 and Fig. 8). Simultaneously, the occurrence of premature rupture in the 19 μm diameter PVA fibres and the relatively low bond strength of the 200 μm diameter PVA fibres resulted in the formation of only a single crack in the samples during the flexural test, as mentioned in Section 4.2. This restriction consequently limited the enhancement of TGH and the ductility of the foam concrete. Hence, a suitable reduction in the bond strength of 19 μm diameter fibres to increase their pull-out length may prolong their working time and enhance the foam concrete's toughness. This could be achieved by appropriate fibre surface treatment, such as physical coating treatment [42–44]. Additionally, D_{90} was another crucial factor influencing PCS and TGH (as shown in Fig. 13c and Fig. 13d). As mentioned earlier, more extensive pores (higher D_{90}) correspond to more defects, promoting crack propagation and thus compromising the foam concrete's post-crack behaviour.

Table 6
Optimal values of hyperparameters of GPR models.

Model	Hyperparameters			
	Basis function	Kernel function	Kernel scale	β
GPR-STS	Constant	Nonisotropic Matern 3/2	286.4155	0.0004
GPR-FCS	Zero	Nonisotropic Rational Quadratic	6.9048	18.6229
GPR-PCS	Zero	Nonisotropic Matern 3/2	3.0948	0.0125
GPR-TGH	Zero	Nonisotropic Matern 3/2	3.6678	2.2102

Interestingly, compared to FC, AR, and D_{90}, FD did not exert a significant influence on PCS and TGH (as depicted in Fig. 13c and Fig. 13d). This suggests that the impact of fibres on the foam concrete's post-crack behaviour was substantial and had already surpassed the effect of FD. Specifically, even small FC significantly improved the foam concrete's post-crack behaviour, particularly for 800 kg/m^3 foam concrete. As

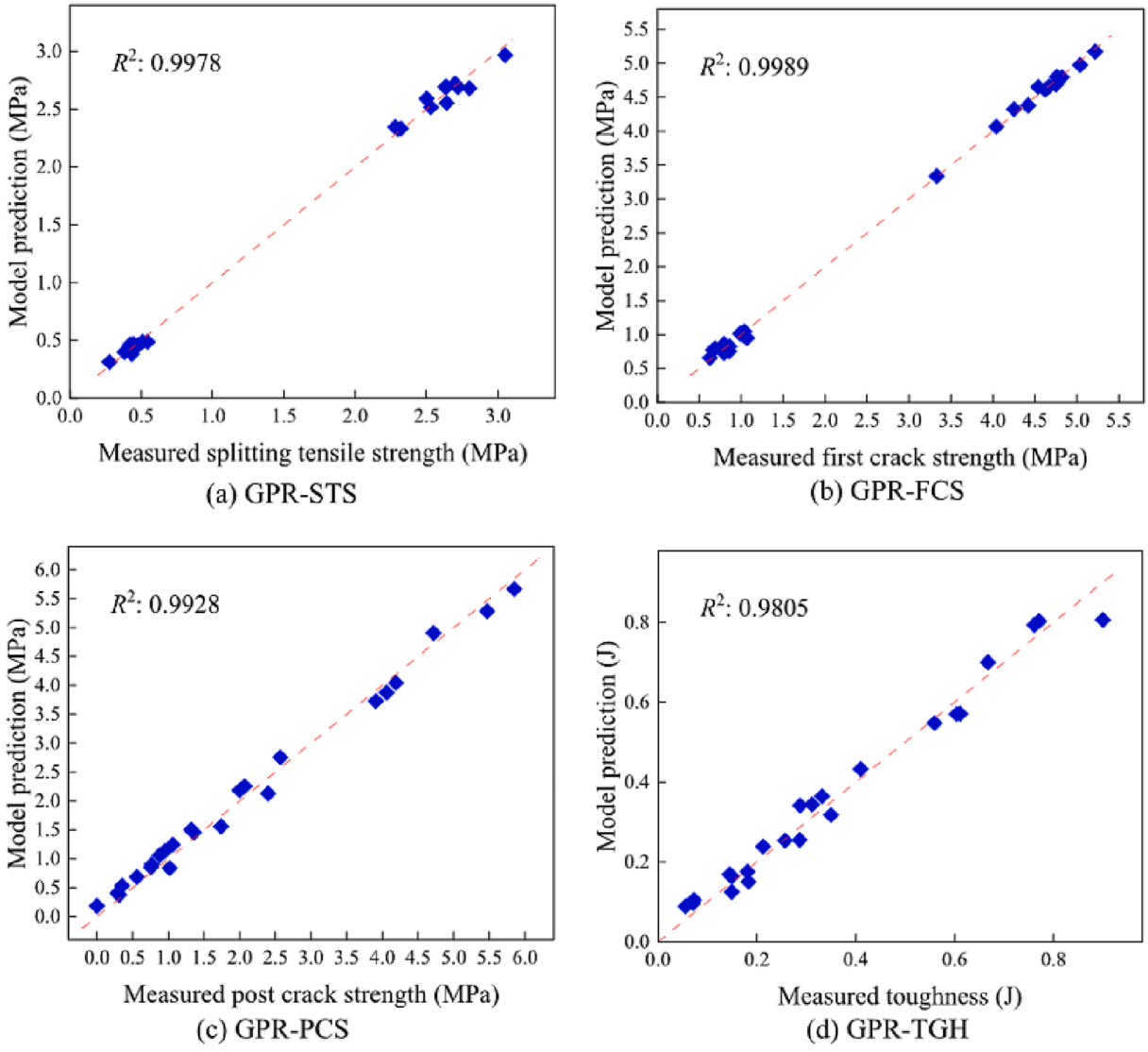

Fig. 12. Regression analysis of GPR models to predict different mechanical properties of foam concrete.

shown in Fig. 8, only 0.15% fibre content was sufficient to provide obvious strain-hardening behaviour for the specimens. Furthermore, as illustrated in Fig. 7a and Fig. 8a, the rate of force decline after the post-crack peak value was lower in 800 kg/m^3 foam concrete than in 1700 kg/m^3 foam concrete. This is due to the longer pull-out length of 19 μm diameter fibres in 800 kg/m^3 foam concrete than in 1700 kg/m^3 foam concrete (as mentioned in 4.3.2 and shown in Fig. 11c and Fig. 10c), enabling fibres to bridge wider cracks in the bending tests of 800 kg/m^3 foam concrete. Therefore, it is economical to incorporate fibres in foam concrete, particularly with low density, to enhance its post-crack behaviour.

6. Conclusion

This paper investigated the effects of several design parameters of foam concrete, including foam concrete density, fibre length, diameter, and content, on its tensile behaviour, including splitting and flexural tensile behaviour. In addition, machine learning technology (GPR and SHAP) was employed to understand the mechanism of fibre influence on tensile behaviour. Using this technology, the significance of each parameter, including design parameters, fibre distribution, and pore structure, for the foam concrete's tensile behaviour was investigated. Furthermore, the fibre failure mode in flexural tests and the flexural force–displacement curves were studied to better understand how important parameters influenced the foam concrete's tensile behaviour. The study's key findings are summarised as follows.

In the flexural bending test, the small-diameter fibres (19 μm) demonstrated strain-hardening behaviour in both low (800 kg/m^3) and high (1700 kg/m^3) density foam concrete. However, they experienced a rupture failure that caused a decline in force after the post-crack peak force. This force drop was more pronounced in high-density foam concrete due to the shorter pull-out length of fibres (i.e., premature fibre rupture under flexural stress compared to the low-density foam concrete). Therefore, reducing the bond strength of small-diameter fibres prolongs the pull-out length and thus could potentially enhance the post-crack flexural behaviour of fibre-reinforced foam concrete. The large-diameter (200 μm) fibres exhibited pull-out failure (low bond strength) in both high- and low-density foam concretes, resulting in a low post-crack force level. However, in low-density foam concrete, most failures occurred inside the cementitious matrix rather than between fibres and the matrix. Hence, enhancing the bond strength of large-diameter fibres in low-density foam concrete would not be beneficial.

According to SHAP's findings, the foam concrete's splitting tensile strength (STS) and first crack flexural strength (FCS) were primarily governed by foam concrete density (FD), D_{90}, and pore shape factor (PSF). In other words, lower FD (corresponding to a higher volume of

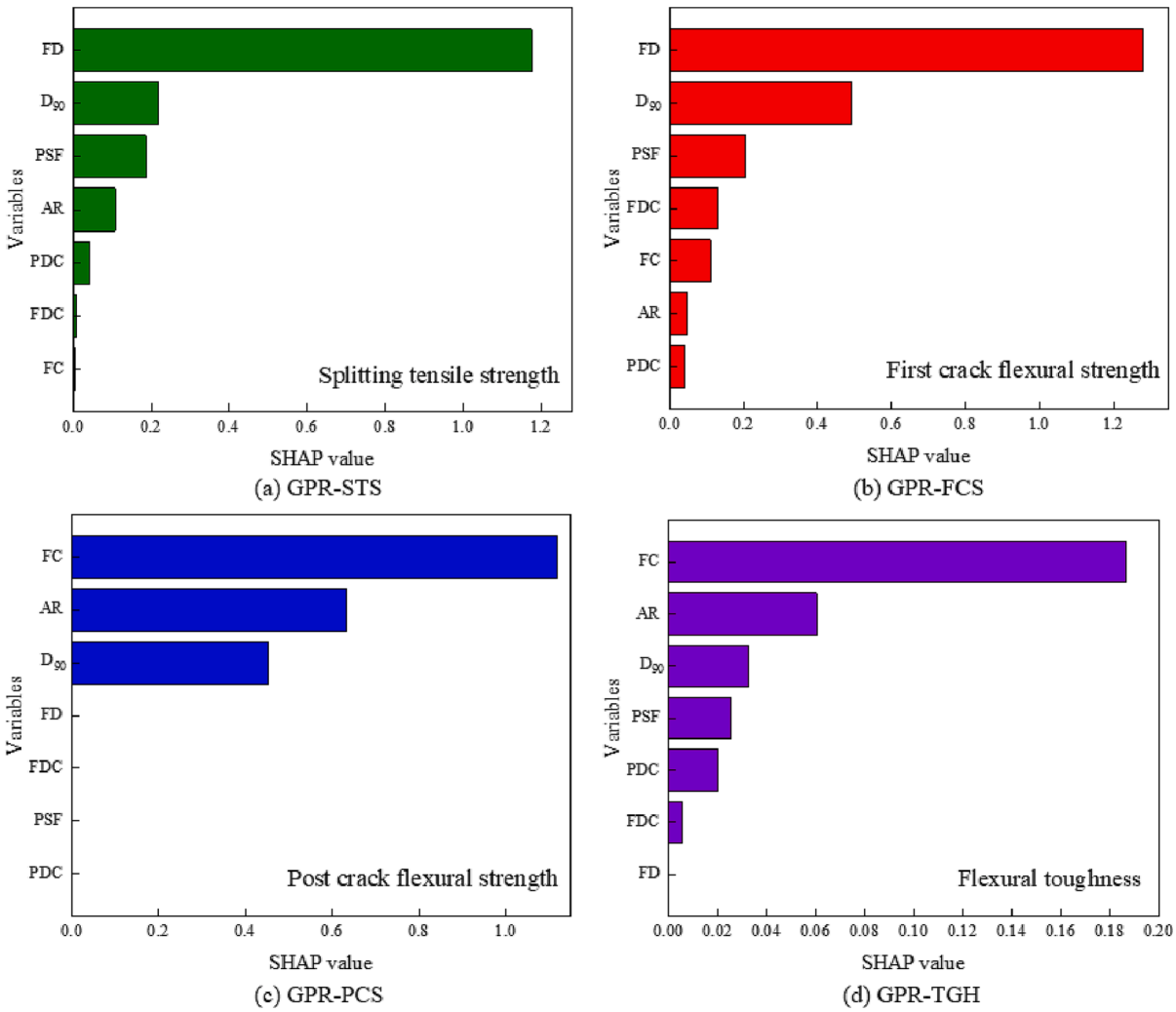

Fig. 13. SHAP analysis of different GPR models.

pores), higher D_{90} (indicating more large pores), and lower PSF (representing more irregular pores) promoted crack initiation and development, resulting in a decrease in the foam concrete's STS and FCS. The enhancements of STS and PSF in foam concrete, attributed to the fibres, were primarily realised through the improvement of the pore structure rather than the fibres' inherent properties. In contrast, normalweight concrete, characterised by its considerable density and reduced porosity in comparison to foam concrete, obtains its STS and FCS enhancements exclusively from the fibres themselves, resulting in more modest improvements. Through optimisation of fibre size and content, the STS and FCS of high-density foam concrete were increased by 75.3% and 28.9%, respectively. The STS and FCS of low-density foam concrete were improved by 49.9% and 71.2%, respectively.

In contrast to the pre-crack behaviour, which was heavily influenced by the pore structure, the post-crack behaviour of foam concrete (i.e., PCS and TGH) were primarily affected by the fibres. Based on the SHAP analysis, the foam concrete's PCS and TGH were mainly governed by fibre content (FC), aspect ratio (AR), and D_{90} (with FC and AR being the most influential factors). Specifically, higher FC and higher AR (which primarily refer to a lower diameter) can more effectively bridge cracks and restrict their development, resulting in an increase in the PCS and TGH of the foam concrete. If the flexural strength is calculated using the ultimate peak force, the addition of fibres can increase it by up to 44.4% and 117.9% in high- and low-density foam concrete, respectively.

In light of the premature rupture of the low-diameter PVA fibres and the limited occurrence of cracks during the flexural test, future investigations may explore appropriate fibre treatment methods to reduce the bond strength between PVA fibres and foam concrete. This would prolong the working time of the fibres and enhance the toughness and ductility of the fibre-reinforced foam concrete. Additionally, further experiments can be conducted to refine the GPR model for improved accuracy and reliability in future studies.

CRediT authorship contribution statement

Jiehong Li: Conceptualization, Data curation, Formal analysis, Investigation, Methodology, Validation, Visualization, Writing – original draft. **Yang Yu:** Formal analysis, Investigation, Methodology. **Taehwan Kim:** Formal analysis, Funding acquisition, Investigation, Methodology, Supervision, Validation, Writing – review & editing. **Ailar Hajimohammadi:** Conceptualization, Formal analysis, Funding acquisition, Investigation, Methodology, Resources, Project administration, Supervision, Validation, Writing – review & editing.

Declaration of Competing Interest

The authors declare that they have no known competing financial interests or personal relationships that could have appeared to influence the work reported in this paper.

Data availability

Data will be made available on request.

Acknowledgements

The authors would like also to acknowledge the support provided by the academic start-up fund from the faculty of engineering at the UNSW Sydney.

References

[1] Y.H.M. Amran, N. Farzadnia, A.A. Abang Ali, Properties and applications of foamed concrete; a review, Constr. Build. Mater. 101 (2015) 990–1005.
[2] A. Raj, D. Sathyan, K.M. Mini, Physical and functional characteristics of foam concrete: A review, Constr. Build. Mater. 221 (2019) 787–799.
[3] E.P. Kearsley, P.J. Wainwright, The effect of porosity on the strength of foamed concrete, Cem. Concr. Res. 32 (2) (2002) 233–239.
[4] N. Mohamad, M.A. Iman, M.A. Othuman Mydin, A.A.A. Samad, J.A. Rosli, A. Noorwirdawati, Mechanical properties and flexure behaviour of lightweight foamed concrete incorporating coir fibre, IOP Conf. Ser.: Earth Environ. Sci. 140 (2018), 012140.
[5] C. Bing, W. Zhen, L. Ning, Experimental research on properties of high-strength foamed concrete, J. Mater. Civ. Eng. 24 (1) (2012) 113–118.
[6] A.A. Jhatial, G.W. Inn, N. Mohamad, U. Johnson Alengaram, K. Hung Mo, R. Abdullah, Influence of polypropylene fibres on the tensile strength and thermal properties of various densities of foamed concrete, IOP Conf. Ser.: Mater. Sci. Eng. 271 (2017), 012058.
[7] A. Baranova, A. Bobrova, Heat-insulating foam concrete based on microsilica reinforced with fiber, IOP Conf. Ser.: Mater. Sci. Eng. 667 (2019), 012009.
[8] S. Wang, J.L.G. Lim, K.H. Tan, Performance of lightweight cementitious composite incorporating carbon nanofibers, Cem. Concr. Compos. 109 (2020), 103561.
[9] J.F. Castillo-Lara, E.A. Flores-Johnson, A. Valadez-Gonzalez, P.J. Herrera-Franco, J.G. Carrillo, P.I. Gonzalez-Chi, Q.M. Li, Mechanical properties of natural fiber reinforced foamed concrete, Materials (Basel) 13 (14) (2020) 3060.
[10] H. Awang, M.A.O. Mydin, A.F. Roslan, Effects of fibre on drying shrinkage, compressive and flexural strength of lightweight foamed concrete, Adv. Mat. Res. 587 (2012) 144–149.
[11] L.M. Vesova, Disperse reinforcing role in producing non-autoclaved cellular foam concrete, Procedia Eng. 150 (2016) 1587–1590.
[12] A.A. Jhatial, W.I. Goh, N. Mohamad, T.A. Rind, A.R. Sandhu, Development of thermal insulating lightweight foamed concrete reinforced with polypropylene fibres, Arab. J. Sci. Eng. 45 (5) (2020) 4067–4076.
[13] R. Brown, A. Shukla, K.R. Natarajan, Fiber reinforcement of concrete structures, 2002.
[14] H.K. Lee, S.Y. Song, Performance characteristics of lightweight aggregate cellular concrete containing polypropylene fibers, J. Reinf. Plast. Compos. 29 (6) (2009) 883–898.
[15] F. Grzymski, M. Musiał, T. Trapko, Mechanical properties of fibre reinforced concrete with recycled fibres, Constr. Build. Mater. 198 (2019) 323–331.
[16] Z.M. Jaini, R.H.M. Rum, K.H. Boon, Strength and fracture energy of foamed concrete incorporating rice husk ash and polypropylene mega-mesh 55, IOP Conf. Ser.: Mater. Sci. Eng. 248 (2017), 012005.
[17] Y.H. Mugahed Amran, R. Alyousef, H. Alabduljabbar, M.H.R. Khudhair, F. Hejazi, A. Alaskar, F. Alrshoudi, A. Siddika, Performance properties of structural fibred-foamed concrete, Results Eng. 5 (2020), 100092.
[18] M. Sun, J. Zhu, T. Sun, Y. Chen, X. Li, W. Yin, J. Han, Multiple effects of nano-CaCO3 and modified polyvinyl alcohol fiber on flexure–tension-resistant performance of engineered cementitious composites, Constr. Build. Mater. 303 (2021) 124426.
[19] H.R. Pakravan, T. Ozbakkaloglu, Synthetic fibers for cementitious composites: A critical and in-depth review of recent advances, Constr. Build. Mater. 207 (2019) 491–518.
[20] B. Raj, D. Sathyan, M.K. Madhavan, A. Raj, Mechanical and durability properties of hybrid fiber reinforced foam concrete, Constr. Build. Mater. 245 (2020), 118373.
[21] L. Yu, Z. Liu, M. Jawaid, E.-R. Kenawy, Mechanical properties optimization of fiber reinforced foam concrete, MATEC Web of Conferences 67 (2016) 03022.
[22] T. Simões, H. Costa, D. Dias-da-Costa, E. Júlio, Influence of fibres on the mechanical behaviour of fibre reinforced concrete matrixes, Constr. Build. Mater. 137 (2017) 548–556.
[23] N. Buratti, C. Mazzotti, M. Savoia, Post-cracking behaviour of steel and macro-synthetic fibre-reinforced concretes, Constr. Build. Mater. 25 (5) (2011) 2713–2722.
[24] Y. Liu, Z. Wang, Z. Fan, J. Gu, Study on properties of sisal fiber modified foamed concrete, IOP Conf. Ser.: Mater. Sci. Eng. 744 (2020), 012042.
[25] A. Amin, S.J. Foster, R.I. Gilbert, W. Kaufmann, Material characterisation of macro synthetic fibre reinforced concrete, Cem. Concr. Compos. 84 (2017) 124–133.
[26] J. Li, A. Hajimohammadi, Y. Yu, B.Y. Lee, T. Kim, Mechanism of PVA fibre influence in foam concrete: from macroscopic to microscopic view, Journal of Materials in Civil Engineering, DOI: 10.1061/JMCEE7/MTENG-16124 (Forthcoming).
[27] H.-V. Mai, M.H. Nguyen, S.H. Trinh, H.-B. Ly, Toward improved prediction of recycled brick aggregate concrete compressive strength by designing ensemble machine learning models, Constr. Build. Mater. 369 (2023) 130613.
[28] Y. Wu, Y. Zhou, Splitting tensile strength prediction of sustainable high-performance concrete using machine learning techniques, Environ. Sci. Pollut. Res. Int. 29 (59) (2022) 89198–89209.
[29] M.-C. Kang, D.-Y. Yoo, R. Gupta, Machine learning-based prediction for compressive and flexural strengths of steel fiber-reinforced concrete, Constr. Build. Mater. 266 (2021) 121117.
[30] W. Ben Chaabene, M. Flah, M.L. Nehdi, Machine learning prediction of mechanical properties of concrete: Critical review, Constr. Build. Mater. 260 (2020) 119889.
[31] Y. Yu, W. Li, J. Li, T.N. Nguyen, A novel optimised self-learning method for compressive strength prediction of high performance concrete, Constr. Build. Mater. 184 (2018) 229–247.
[32] T.N. Nguyen, Y. Yu, J. Li, N. Gowripalan, V. Sirivivatnanon, Elastic modulus of ASR-affected concrete: An evaluation using Artificial Neural Network, Comput. Concr. 24 (6) (2019) 541–553.
[33] D.-K. Bui, T. Nguyen, J.-S. Chou, H. Nguyen-Xuan, T.D. Ngo, A modified firefly algorithm-artificial neural network expert system for predicting compressive and tensile strength of high-performance concrete, Constr. Build. Mater. 180 (2018) 320–333.
[34] J. Xiong, J.-C. He, X.-S. Leng, T.-Y. Zhang, Gaussian process regressions on hot deformation behaviors of FGH98 nickel-based powder superalloy, J. Mater. Sci. Technol. 146 (2023) 177–185.
[35] A. Hajimohammadi, T. Ngo, A. Kashani, Sustainable one-part geopolymer foams with glass fines versus sand as aggregates, Constr. Build. Mater. 171 (2018) 223–231.
[36] ASTM, ASTM C496/C496M-17, Standard test method for splitting tensile strength of cylindrical concrete specimens, US American Standard Testing Method (ASTM), 2017.
[37] ASTM, ASTM C348, Standard test method for flexural strength of hydraulic-cement mortars, US American Standard Testing Method (ASTM), 2019.
[38] A. Noushini, B. Samali, K. Vessalas, Effect of polyvinyl alcohol (PVA) fibre on dynamic and material properties of fibre reinforced concrete, Constr. Build. Mater. 49 (2013) 374–383.
[39] C. Lin, O. Kayali, E.V. Morozov, D.J. Sharp, Influence of fibre type on flexural behaviour of self-compacting fibre reinforced cementitious composites, Cem. Concr. Compos. 51 (2014) 27–37.
[40] M. Vega García, J.L. Aznarte, Shapley additive explanations for NO2 forecasting, Eco. Inform. 56 (2020) 101039.
[41] A.A. Hilal, N.H. Thom, A.R. Dawson, On entrained pore size distribution of foamed concrete, Constr. Build. Mater. 75 (2015) 227–233.
[42] M.F. Arain, M. Wang, J. Chen, H. Zhang, Study on PVA fiber surface modification for strain-hardening cementitious composites (PVA-SHCC), Constr. Build. Mater. 197 (2019) 107–116.
[43] M.F. Arain, M. Wang, J. Chen, H. Zhang, Experimental and numerical study on tensile behavior of surface modified PVA fiber reinforced strain-hardening cementitious composites (PVA-SHCC), Constr. Build. Mater. 217 (2019) 403–415.
[44] C. Ding, L. Guo, B. Chen, Z. Deng, G. Huang, D. Luo, Alkali resistance and surface modification of high strength and high modulus PVA fibers, J. Chin. Ceram. Soc. 47 (2) (2019) 228–235.